▌ Organometallic Chemistry

Chain-Conformation-Directed Polymerization Cyclization for Effective Synthesis of Macrocycles in Bulk

Kai Cao+,[a] Liao Peng+,[a, b] Junli Zhu+,[c] Anchao Feng,[d] Dapeng Liu,[a] Aklilu Worku,[a] Senyang Liu,[b] Jiaping Lin,*[c] Jinying Yuan,*[b] and Xiaosong Wang*[a]

Abstract: Biological cyclization is highly efficient, and this can be attributed to the conformation of the backbone of the biopolymer. Taking advantage of metal-coordination geometry, we developed a method for conformation-directed polymerization cyclization through rational design of metal carbonyl monomers that could be used to produce cyclic macromolecules, even in bulk. ^PFpR [$^PFp=$ $(PPh_2(CH_2)_3Cp)Fe(CO)_2$ with the phosphine group tethered on the cyclopentadiene (Cp) ring; $R=CH_3$ or $(CH_2)_5CH_3$] was designed and synthesized for migration insertion polymerization to generate P(^PFpR) with the polymer backbone containing Cp—Fe bonds. Growth of the backbone led to a cyclic conformation with close end-to-end distances, which facilitated the cyclization. This conformation-directed cyclization was attributed to the piano-stool metal-coordination geometry of the repeating units and the low rotational barrier of the Cp—Fe bonds in the backbone. The produced macrocycles, which contain a metal carbonyl coordination structure in their backbones, are rigid, unlike many organic macrocycles. The macrocycles thus have a large excluded volume. This new type of metal carbonyl macrocycle will be of interest as a building block for supramolecular chemistry and in the exploration of novel materials.

Introduction

The conformation of biopolymers is important for many biological processes, including the cyclization of polypeptides.[1] Biosynthesis has inspired chemists to develop methods for the conformation-directed ring closure of polypeptides[2] and macromolecules,[3] which are usually achieved through the preorganization of chains in solution.[4] However, the products are often contaminated by unreacted linear precursors,[5] and tedious purification steps are required in many cases to isolate the macrocycles.[6] Ring-expansion polymerization is more effective in the synthesis of macrocycles, as it forces the growth of the polymer chain within a ring structure through the insertion of monomers into activated cyclic chains.[7] However, the synthesis of cyclic initiators is not trivial, and the polymerization often generates a small amount of linear analogues as well.[7b] In addition to ring closure and expansion, it is also possible to grow linear polymer chains into macrocycles.[5c, 8] This polymerization cyclization is attributed to the conformation of the polymer chain, but it is less studied than other routes. By taking advantage of the metal coordination geometries[9] and the nature of coordination bonds, main-chain organometallic polymers are ideal systems to explore conformation-directed polymerization cyclization.[8]

We developed migration insertion polymerization (MIP) that can polymerize FpP [Fp=CpFe(CO)₂, Cp=cyclopentadiene; P=alkyldiphenylphosphine][10] and other metal carbonyl monomers[11] under a step-growth mechanism[12] to generate P(FpP) and its analogues (Figure 1a).[13] One interesting feature of P(FpP) is the piano-stool metal coordination geometry of the repeating units,[13] which is nonlinear and accounts for various chain conformations depending on the solution conditions and the backbone structures.[11, 14] The MIP of FpP in either bulk or THF generates extended P(FpP) chains with NMR spectroscopy detectable end groups (Figure 1a).[10b, 12, 13, 15] This linear growth is attributed to the directional Fe—C and Fe—phosphine metal coordination bonds that extend the chains and prevent intramolecular reaction of the end groups for cyclization.

It is well known that the Cp—Fe coordination bond has a low rotational barrier.[16] The incorporation of this bond into

[a] Dr. K. Cao,+ L. Peng,+ D. Liu, A. Worku, Prof. X. Wang
Department of Chemistry, Waterloo Institute for Nanotechnology
University of Waterloo, Waterloo, ON, N2L 3G1 (Canada)
E-mail: xiaosong.wang@uwaterloo.ca

[b] L. Peng,+ S. Liu, Prof. J. Yuan
Key Laboratory of Organic Optoelectronics & Molecular Engineering
Department of Chemistry, Tsinghua University, 100084 Beijing (P. R. China)
E-mail: yuanjy@mail.tsinghua.edu.cn

[c] J. Zhu,+ Prof. J. Lin
Shanghai Key Laboratory of Advanced Polymeric Materials
State Key Laboratory of Bioreactor Engineering, Key Laboratory for
Ultrafine Materials of Ministry of Education, School of
Materials Science and Engineering, East China University of Science and
Technology, Shanghai, 200237 (P. R. China)
E-mail: jlin@ecust.edu.cnf

[d] Prof. A. Feng
College of Materials Science and Engineering
Beijing University of Chemical Technology, Beijing 100029 (P. R. China)

[+] These authors contributed equally to this work.

Supporting Information and the ORCID identification number(s) for the author(s) of this article can be found under:
https://doi.org/10.1002/chem.201803471.
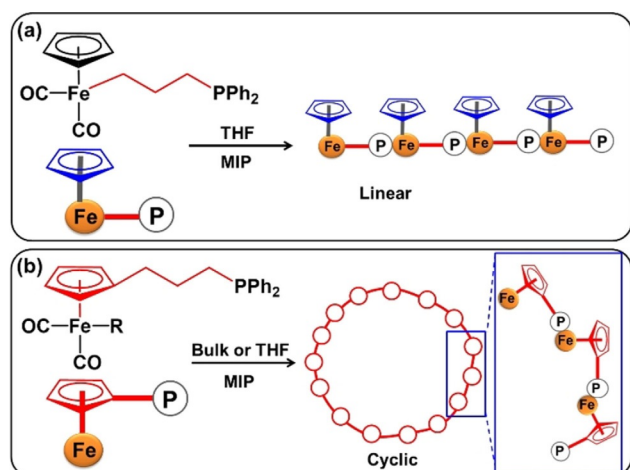
Figure 1. Chemical structures of: a) FpP, and b) PFpR and schematic illustration of the monomers and corresponding: a) linear P(FpP), and b) cyclic P(PFpR) resulting from migration insertion polymerization (MIP). The bonds highlighted in red represent those in the main chains.

Scheme 1. Schematic illustration for the synthesis of PFpR.

Figure 2. a) ^{13}C NMR (C_6D_6), b) ^{1}H NMR (CDCl$_3$), and c) ^{31}P NMR (CDCl$_3$) spectra of **1b**. In panel a, the J_{CP} for the β carbon atom is larger than that for the α carbon atom, which is usually observed for phosphorus compounds.[18]
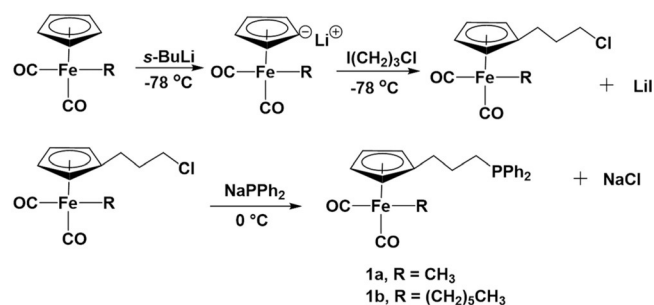
the backbone to replace the Fe–C bonds in P(FpP) will render the resultant chain rotatable[8] and will encourage the chain to adopt a conformation with close end-to-end distances for effective polymerization cyclization.[8] To explore this conformation-directed synthesis, we designed PFpR [PFp = (PPh$_2$(CH$_2$)$_3$Cp)Fe(CO)$_2$, R = CH$_3$, (CH$_2$)$_5$CH$_3$] monomers for MIP. This design, in which the phosphine group is tethered onto the Cp ring, allows for the MIP to yield a polymer backbone with Cp–Fe bonds.

Herein, we report the synthesis and MIP of PFpR, which is a step-growth polymerization.[12] A traditional step-growth polymerization tends to produce small rings in dilute solution, but this can be suppressed by increasing the concentrations of the monomers. However, the MIP of PFpR generated P(PFpR) macrocycles without linear contaminants, even if the polymerization was performed in bulk. An all-atom dynamic simulation indicated that the coordination geometry and bonds of PFpR accounted for the cyclic conformation of P(PFpR). The resultant macrocycles with metal coordination bonds are rigid, have large excluded volumes (EVs) (Figure 1), and represent a new group of ring molecules.
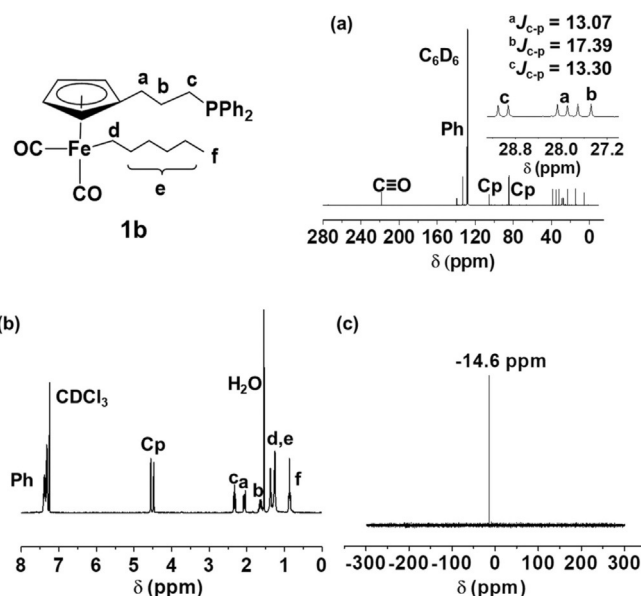
Results and Discussion

Synthesis and characterization of PFpR (1)

PFpR was synthesized (Scheme 1) and characterized by FTIR and NMR spectroscopy. Taking **1b** [R = (CH$_2$)$_5$CH$_3$] as an example, the presence of terminal CO groups is indicated by the FTIR absorption bands at $\tilde{v}$ = 1997 and 1935 cm^{-1} (Figure S2 in the Supporting Information)[10b] and is confirmed by the ^{13}C NMR spectrum (Figure 2a), which shows a chemical shift at δ = 218.7 ppm due to the CO groups.[12] All other assignments of the signals in Figure 2a are confirmed by the $^{13}C,^{1}H$ HMQC 2D NMR spectrum (HMQC: heteronuclear multiple quantum correlation, Figure S3a). Figure 2b displays the ^{1}H NMR spec-

trum of **1b**. As shown in this figure, the signals at δ = 4.6 and 4.5 ppm can be attributed to the protons in the Cp ring,[17] and those at δ = 7.5–7.0 ppm can be assigned to the phenyl groups. Other assignments (a–e) as marked in Figure 2b are confirmed by the $^{1}H,^{1}H$ COSY 2D NMR spectrum (Figure S3b). The proton integration ratio for Ph/Cp/a/b/c/(d+e)/f is 10:4:2:2:2:10:3, which matches the theoretical values for the targeted structure. The ^{31}P NMR spectrum (Figure 2c) shows a single resonance at δ = −14.6 ppm, which is indicative of the presence of a phosphine.[10b] The mass of **1b** was determined by using electrospray ionization mass spectrometry, which showed an ion with m/z = 489 (Figure S4) corresponding to [M+H]$^+$ of **1b**. The C/H/Fe ratio found by elemental analysis also matches the theoretical value (Table S1). The chemical structure of **1a** was characterized and confirmed by the same techniques (Table S1, Figure S5a,b, and Figures S6–S8).

MIP cyclization of PFpR (1) for c-P(PFpR) (2)

Bulk MIP of **1** at 105 °C was first performed. The oil-like monomer gradually became a transparent reddish-brown solid

during the MIP. After 48 h, the polymerization was terminated by cooling the reaction flask to 23 °C. The crude product was dissolved in a small amount of THF, which generated a clear red solution. This THF solution was added dropwise to *n*-hexane, a poor solvent, to yield a yellow precipitate. Compound **2** is soluble in a broad range of organic solvents (Table S2), including toluene, THF, and DMF, and is chemically stable in C_6D_6 for 1 week, as indicated by ^1H NMR and ^{31}P NMR spectroscopy (Figure S9). Differential scanning calorimetry (DSC) (Figure S10 a, c) and powder X-ray diffraction (Figure S11) indicate that **2** possesses no melting temperature and is amorphous. The glass transition temperature (T_g) of **2 a** and **2 b** are 93 and 70 °C, respectively. The higher T_g of **2 a** is due to the smaller free volume resulting from the smaller pendant methyl group. Thermogravimetric analysis (TGA) (Figure S10 b, d) reveals that **2 a** and **2 b** are thermally stable up to 162 and 173 °C, respectively.

The chemical structure of **2** was analyzed by FTIR and NMR spectroscopies (Figures S5 c, d and S12–S14). The FTIR spectrum (Figure S12) of **2 b** shows two absorption bands at $\tilde{\nu} = 1906$ and 1601 cm^{-1} corresponding to the terminal and acyl CO groups, respectively.[10b] These two CO groups are also detectable in the ^{13}C NMR spectrum (Figure 3 a) with signals at $\delta = 273.9$ and 220.7 ppm, respectively. The appearance of a cross peak in the $^{13}C,^1H$ HMBC 2D NMR spectrum (HMBC: heteronuclear multiple bond correlation, Figure S13 a) confirms that the signal at $\delta = 273.9$ ppm is the acyl group with a CH$_2$ group α to the carbon atom. The appearance of the acyl group indicates that **2 b** is produced from MIP.[10b]

The ^1H NMR spectrum (Figure 3 b) of **2 b** displays corresponding assignments for the protons in propyl diphenylphosphine (signals Ph, a, b, and c in Figure 3 b) and Cp groups (signal Cp in Figure 3 b). These two groups, by coordination to Fe, constitute the backbone of **2 b*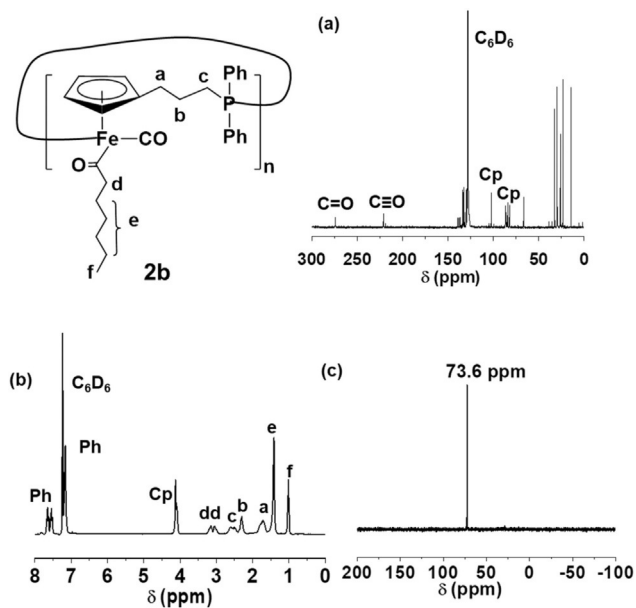* (Figure 1 b). The protons due to the pendent acyl groups are assigned as signals d, e, and f in Figure 3 b. These assignments are confirmed by the $^{13}C,^1H$ HMQC 2D NMR spectrum (Figure S13 b). The appearance of two diastereotopic protons (signals d in Figure 3 b), ascribed to the CH$_2$ group α to the acyl CO group, further confirms the occurrence of MIP.[10b] It is noticeable that only one resonance signal ($\delta = 4.1$ ppm) due to the Cp groups is observed in the ^1H NMR spectrum (Figure 3 b). The ^{31}P NMR spectrum of **2 b** (Figure 3 c) also shows a single resonance at $\delta = 73.6$ ppm due to the main-chain-coordinated phosphorus atom. This suggests that **2 b** possesses no unreacted Fp or uncoordinated phosphine end groups[10b] (Figure S16 a, b). Compound **2 b** is, therefore, a macrocycle.[14] Further experiments indicate that the MIP of both **1 a** and **1 b** in either bulk or THF generates corresponding **2 a** and **2 b** without detectable end groups (Figures S5 c, S14, and S15). The MIP of ^PFpR is, therefore, a cyclization process and c-P(^PFpR) is produced.[14]

Kinetic studies were performed to understand the cyclization process. The ^{31}P NMR spectra of the samples taken at different times during the MIP of **1 a** at 105 °C are illustrated in Figure 4
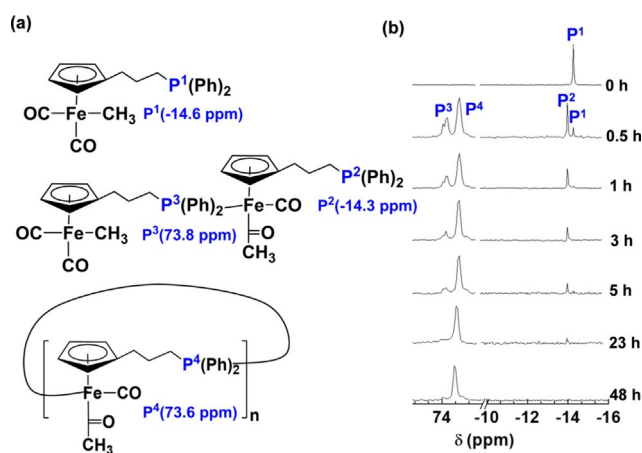

Figure 4. a) Chemical structures of the starting monomers and resulting products, including oligomers and macrocycles, during MIP. The dimer drawn in the figure represents oligomers. b) ^{31}P NMR spectra of the crude products taken at different time intervals during the MIP of **1 a** in bulk at 105 °C.

(the samples are crude products without purification by precipitation), in which four chemical shifts are detected and labeled as P^1, P^2, P^3, and P^4. Signal P^1 is attributed to the phosphorus atom in monomer **1 a** (Figures 2 c and S7). Signals P^2 and P^3 are assigned to the phosphorus atom in the linear oligomers on the basis of our previous work on *l*-P(FpP).[12] This assignment is confirmed by the ^{31}P NMR spectra of the oligomers and macrocycles separated from the crude products (Figure S17). Signal P^4 is assigned to the phosphorus atom in macrocycle **2 a** (Figures 3 c and S14). The spectra of the final crude product (Figure 4) and the precipitation-purified sample (Figure S14) show the same single signal (P^4), which suggests that the macrocycles are produced as the only products.

Integration of the ^{31}P NMR spectrum was also performed to estimate the conversion of the monomer.[12] As shown in

Figure 3. a) ^{13}C NMR (C_6D_6), b) ^1H NMR (C_6D_6), and c) ^{31}P NMR (CDCl$_3$) spectra of **2 b**.

Figure 4, the polymerization consumes approximately 94.9% of the monomers after 0.5 h. The resultant products contain 50% macrocycles (P^4) and 50% linear oligomers (P^2 and P^3). This result suggests that the cyclization has a fast rate, as macrocycle **2a** is produced within 0.5 h. The linear oligomers are completely converted into macrocycle **2a** after a longer time period (48 h), which is attributed to the slow diffusion of the oligomers in the bulk matrix of the macromolecule. This MIP cyclization is directed by the conformation of the chain, as designed, and this may occur even the mobility of the polymer chain is low during the bulk polymerization. To test this idea, we performed the MIP of **1a** at 70 °C, a temperature that is lower than the T_g of **2a** (93 °C). Cyclization still occurred and produced macrocycle **2a** (Figure S18a). The cyclization, therefore, benefits more from the conformation of the polymer chain than from the mobility of the chain.

The MIP of **1b** at either 70 or 105 °C underwent a similar cyclization process to produce **2b** (Figure S18b, c). The polymerization rates for **1b** are much faster than those for **1a** at the same temperature, because the chain mobility of **2b** ($T_g = 70$ °C) is higher than that of **2a** ($T_g = 97$ °C). For example, monomer **1b** was completely converted into macrocycle **2b** within 3 h if the polymerization was performed in bulk at 105 °C.

Molecular weight and ring structure of 2

The gel-permeation chromatography (GPC) measurements indicate that the apparent number-average molecular weight ($M_{n,GPC}$) relative to the polystyrene (PS) standard are 8900 and 14100 g mol^{-1} for **2a** and **2b**, respectively. The absolute weight-average molecular weights, as determined by static light scattering (SLS) ($M_{w,SLS}$, Table S3), are 9900 and 15000 g mol^{-1}, respectively. The GPC and SLS results both confirm that compounds **2** are macromolecules. On the basis of the $M_{w,SLS}$ values, the values for the degree of polymerization (DP) of **2a** and **2b** are 24 and 31, respectively. This relatively small DP is due to cyclization directed by the chain conformation. A long fiber can be pulled out from compounds **2** at a temperature above their T_g (Figure S19), which suggests that the macrocycles, despite the small DP, have viscoelastic properties.

The cyclic voltammetry (CV) curves (Figure S20a) of **2b**, similar to those of the P(FpP) linear analogues (Figure S20b), show two anodic potentials at 0.75 and 0.99 V due to the oxidation of the Fp units,[19] because the iron atoms adjacent to the oxidized Fp groups have a higher oxidation potential.[20] It was reported that the CV curve of cyclic polyferrocenylsilane (c-PFS) with an odd number of repeating units displays a three-wave pattern for the oxidation processes. This effect of the ring structure on the redox behavior, however, only occurs for rings with a small DP (DP = 2–7).[8] The size of **2b** (DP = 31) is relatively large, and the spatial effect due to the ring structure is negligible.

The cyclic structure of **2** was analyzed by transmission electron microscopy (TEM) and atomic force microscopy (AFM) techniques. Ring molecules, especially those with flexible back-

bones, are usually difficult to image. Only those rings with grafted polymer brushes have previously been imaged.[7b, 21] The ring structure of **2** restricts rotation of the Fp–Cp metal coordination bonds, so the macrocycle is rigid. We believed that this rigidity and the high electron density resulting from the metal elements would allow for characterization by microcopy,[22] so we examined the possibility to image the cyclic polymers directly. The TEM specimen was prepared by blotting a drop of solution containing **2b** on a carbon film. Figure 5a displays the TEM image, which reveals a cyclic structure. Nota-
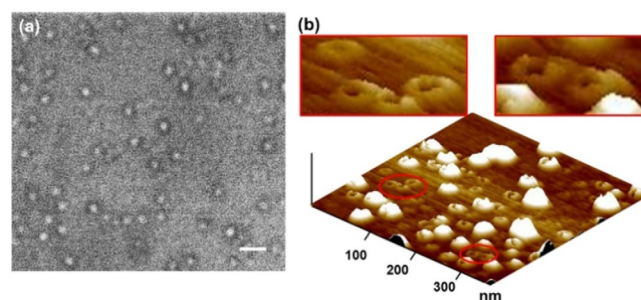
Figure 5. a) TEM (scale bar = 50 nm), and b) AFM images of macrocycles. Insets show the enlargements of the areas highlighted by red circles.

bly, the molecule was not discernible upon initial placement of the sample in the TEM chamber. However, after a few minutes, we noticed rupture of the carbon film, which resulted in ring structures with bright centers. The average diameter (D) of the rings is approximately 15 nm. If the rings are macrocycles, the DP is estimated to be 36 (SI) by comparing the perimeter with the theoretical size of the monomer. This value is close to the $M_{w,SLS}$ of **2b** (Table S3), which suggests that the rings appearing in the TEM image represent macrocycles. The success of this TEM image is rationalized by the uneven stress on the carbon film upon interaction of the rigid molecule with the substrate.[23] As a result, the film at the central area of the ring becomes fragile and breaks after a long ($\approx$3 mins) exposure to the electron beam, which results in the contrast that facilitates the TEM experiment. Figure 5b displays an AFM topographic image of **2b**. A drop of the solution was naturally dried on a mica substrate for the measurement, so the molecules may have aggregated during the drying process to result in large aggregates (Figure 5b). Nevertheless, a few individual objects with donut-like morphology can be observed, which supports the ring structure of the macrocycles.

Cyclic polymers in good solvents, in comparison with their linear analogues, are expected to have large excluded volumes (EVs).[24] The ratio of D_g/D_h (D_g = radius of gyration D_h = hydrodynamic radius) is an indicator of the EV, because D_g is more sensitive to EV than D_h.[24b] Macrocycles with flexible backbones, for example, cyclic polystyrene, have small D_g/D_h ratios in the range of 0.8 to 1.2, as reported in the literature (Table S4), which suggests that their EVs are small.[24b] In contrast, the D_g/D_h ratios of macrocycles **2a** and **2b** are 4.0 and 4.2 (Table S4), respectively. These larger ratios suggest large EVs, and this can be attributed to the rigid backbone con-
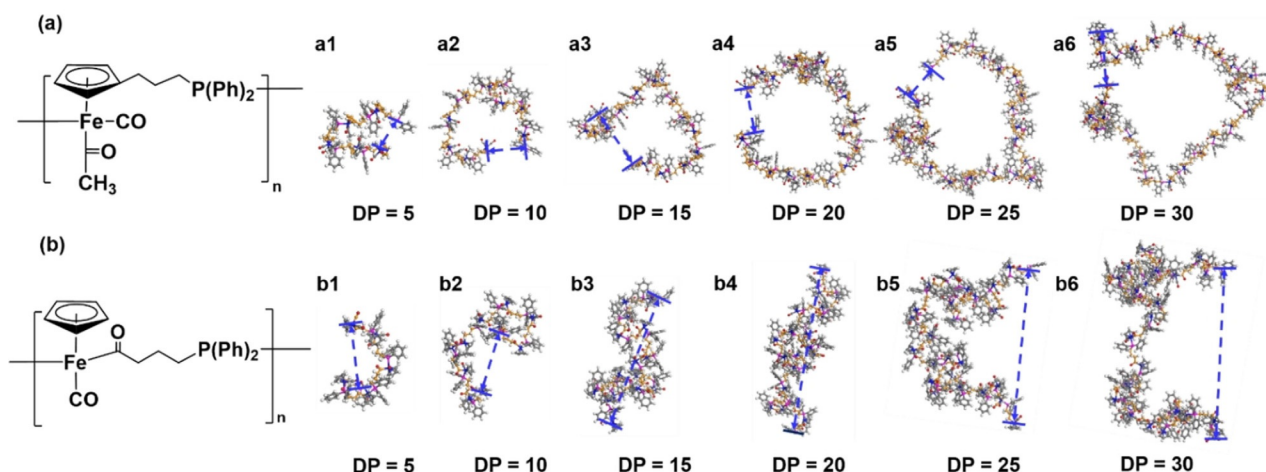
Figure 6. Snapshots resulting from the dynamic simulations of: a) P(^{P}FpR), and b) P(FpP) with the degree of polymerization (DP) varied from 5 to 30 (Fe: blue, P: purple: C in the backbone: yellow, C in the pendent groups: gray).

structed from the metal-coordination structural units. In a recent work, the D_g/D_h ratio for cyclic poly(phenylacetylene) was reported to be approximately 6.7.[25] The alkene backbone of the conjugated macrocycle is expected to be more rigid than that of **2** that contains flexible alkyl spacers. This comparison justifies that the rigidity of the backbone is one factor that influences the EV.

Dynamic simulation of the ^{P}FpR and FpP oligomers

Effective cyclization can be attributed to the chain conformation of the P(^{P}FpR) backbone. To verify this, molecular dynamics simulations of P(^{P}FpMe) were performed. Snapshots of P(^{P}FpMe) with various DPs (5–30) are listed in Figure 6a and are compared with those simulated for the P(FpMe) macromolecules (Figure 6b). As shown in Figure 6a, the P(^{P}FpMe) main chains adopt circular conformations regardless of their DP with root-mean-squared end-to-end distances (R_e) of approximately 15 Å (Figures S22 and S23a). In contrast, the R_e of P(FpP) (Figure 6b) increases from 13.84 to 62.55 Å (Figure S23a) as the DP is varied from 5 to 30. This larger R_e renders the cyclization difficult during the MIP of FpP either in bulk or THF (Figure 6b).[14,26] The circular chain conformation of P(^{P}FpR) is attributed to the incorporation of Cp–Fe bonds in the main chain of the polymer. In addition, the calculations (Figure S23b–f) indicate that the angles between the two vectors of adjacent repeating units in P(^{P}FpMe) is larger than that in P(FpP). This suggests that the design of ^{P}FpR also takes better advantage of the metal coordination geometry for effective MIP cyclization (Figure S23d,f).

Conclusions

In summary, ^{P}FpR (R=methyl or hexyl) with a phosphine group tethered on the Cp ring was designed for MIP, which generated c-P(^{P}FpR) with the main chain containing Cp–Fe bonds. Unlike most reported syntheses of ring molecules,[27] this MIP cyclization can be performed even in bulk, and no ad-

ditional steps are required to purify the macrocycles. The resultant macrocycles have large EVs owing to the rigid metal-coordination backbone. The cyclization is attributed to the conformation of the backbone of the polymer chain and is reminiscent of the biological synthesis of cyclic polypeptides; this protocol creates a new group of metal carbonyl macrocycles for supramolecular chemistry and for the exploration of new materials.[28]

Experimental Section

Synthesis and characterization

General procedure for the synthesis of [η⁵-Cl(CH₂)₃C₅H₄]-Fe(CO)₂R: (η⁵-C₅H₅)Fe(CO)₂R (2.0 mmol) [R=CH₃ or (CH₂)₅CH₃] was dissolved in THF (40 mL). The solution was cooled to −78 °C by using a dry ice/acetone bath, and sBuLi solution (1.4 M) in cyclohexane (1.7 mL, 2.4 mmol) was then added dropwise. The solution gradually turned from yellow to dark red. After stirring at −78 °C for 30 min, 1-chloro-3-iodopropane (3.2 mL, 3.0 mmol) was added dropwise, which generated a green solution. At the end of the addition, the cold bath was removed, and the system was warmed to room temperature. The solution gradually turned brown. After stirring at room temperature for 1.5 h, THF was removed under vacuum to yield a brown oil. The crude product was dissolved in a small amount of n-hexane and was passed through a plug of Celite to remove LiI. The solution was concentrated under vacuum and was subsequently chromatographed on a silica gel column by using n-hexane as the eluent. Unreacted 1-chloro-3-iodopropane eluted first, and this was followed by two yellow bands. The first band was unreacted FpR, and the second yellow band was the product, which was collected. The solvent was finally removed under vacuum to yield a yellow oil as the final product. The yield for the final product with R of CH₃ or (CH₂)₅CH₃ is about 50%.

[η⁵-Cl(CH₂)₃C₅H₄]Fe(CO)₂CH₃: ^{1}H NMR (300 MHz, CDCl₃): δ = 4.65 (t, 2 H, C₅H₄), 4.58 (t, 2 H, C₅H₄), 3.57 (t, 2 H, CH₂Cl), 2.37 (t, 2 H, CH₂C₅H₄), 1.99 (m, 2 H, C₅H₄CH₂CH₂CH₂), 0.14 ppm (s, 3 H, FeCH₃).

[η⁵-Cl(CH₂)₃C₅H₄]Fe(CO)₂(CH₂)₅CH₃: ^{1}H NMR (300 MHz, CDCl₃): δ = 4.63 (t, 2 H, C₅H₄), 4.59 (t, 2 H, C₅H₄), 3.57 (t, 2 H, CH₂Cl), 2.40 (t, 2 H, CH₂C₅H₄), 1.99 (m, 2 H, C₅H₄CH₂CH₂CH₂), 1.43 (m, 10 H, Fe(CH₂)₅), 0.87 ppm (t, 3 H, Fe(CH₂)₅CH₃).

General procedure for the synthesis of [η^5-Ph$_2$P(CH$_2$)$_3$C$_5$H$_4$]-Fe(CO)$_2$R [R=CH$_3$ or (CH$_2$)$_5$CH$_3$]]: [η^5-Cl(CH$_2$)$_3$C$_5$H$_4$]Fe(CO)$_2$R (1.5 mmol) was dissolved in THF (20 mL). The THF solution was cooled to 0 °C by using an ice bath and a THF solution of NaPPh$_2$ (6.0 mL, 0.5 mol L^{-1}) was added dropwise. After the addition, the ice bath was removed. The solution was warmed to room temperature and was subsequently stirred for 2 h. At the end of the reaction, degassed methanol (2.0 mL) was added dropwise to react with the excess amount of NaPPh$_2$. The solution was then passed through a Celite column to remove salts, and the filtrate was concentrated under vacuum. The crude product was chromatographed on a silica gel column by using n-hexane/dichloromethane (3:1, v/v) as the eluent. The yellow band was collected, and the solvents were removed under vacuum to yield a yellow oil as the final product. The yield for the final product with R of CH$_3$ or (CH$_2$)$_5$CH$_3$ is about 47 %.

[η^5-Ph$_2$P(CH$_2$)$_3$C$_5$H$_4$]Fe(CO)$_2$CH$_3$ **(1a)**: ^{1}H NMR (300 MHz, C$_6$D$_6$): δ = 7.30 (m, 5H, C$_6$H$_5$), 7.12 (m, 5H, C$_6$H$_5$), 3.95 (t, 2H, C$_5$H$_4$), 3.86 (t, 2H, C$_5$H$_4$), 1.94 (t, 2H, CH$_2$PPh$_2$), 1.85 (t, 2H, CH$_2$C$_5$H$_4$), 1.44 (m, 2H, CH$_2$CH$_2$CH$_2$PPh$_2$), 0.28 ppm (s, 3H, FeCH$_3$); ^{13}C NMR 75 MHz, C$_6$D$_6$): δ = 218.2 (s, C≡O), 139.5 (s, C$_6$H$_5$), 139.4 (s, C$_6$H$_5$), 133.2 (s, C$_6$H$_5$), 133.0 (s, C$_6$H$_5$), 105.9 (s, C$_5$H$_4$), 84.6 (s, C$_5$H$_4$), 83.6 (s, C$_5$H$_4$), 29.0–28.7 (d, J_{PC} = 13.2 Hz, CH$_2$CH$_2$CH$_2$PPh$_2$), 28.3–27.8 (d, J_{PC} = 13.1 Hz, CH$_2$CH$_2$CH$_2$PPh$_2$), 27.8–27.2 (d, J_{PC} = 17.5 Hz, CH$_2$CH$_2$CH$_2$PPh$_2$), −20.6 ppm (s, FeCH$_3$); ^{31}P NMR (120 MHz, CDCl$_3$): δ = −14.6 ppm. FTIR: $\tilde{v}$ = 1994, 1933 cm^{-1}; MS (ESI): m/z: 419.17 [M+H]$^+$; elemental analysis calcd (%) for C$_{23}$H$_{23}$FeO$_2$P (418.25): C 66.05, H 5.54, Fe 13.35; found: C 66.34, H 6.35, Fe 13.35.

[η^5-Ph$_2$P(CH$_2$)$_3$C$_5$H$_4$]Fe(CO)$_2$(CH$_2$)$_5$CH$_3$ **(1b)**: ^{1}H NMR (300 MHz, CDCl$_3$): δ = 7.50–7.30 (br, 10H, C$_6$H$_5$), 4.56 (t, 2H, C$_5$H$_4$), 4.48 (t, 2H, C$_5$H$_4$), 2.31 (t, 2H, CH$_2$PPh$_2$), 2.02 (t, 2H, CH$_2$C$_5$H$_4$), 1.60 (t, 2H, CH$_2$CH$_2$CH$_2$PPh$_2$), 1.56–1.00 (m, 10H, Fe(CH$_2$)$_5$), 0.87 ppm (s, 3H, Fe(CH$_2$)$_5$CH$_3$); ^{13}C NMR (75 MHz, C$_6$D$_6$): δ = 218.7 (s, C≡O), 139.5 (s, C$_6$H$_5$), 139.4 (s, C$_6$H$_5$), 133.2 (s, C$_6$H$_5$), 133.0 (s, C$_6$H$_5$), 105.5 (s, C$_5$H$_4$), 85.0 (s, C$_5$H$_4$), 84.6 (s, C$_5$H$_4$), 39.9 (s, CH$_2$CH$_2$CH$_2$PPh$_2$), 35.4 (s, FeCH$_2$(CH$_2$)$_4$CH$_3$), 32.3 (s, FeCH$_2$(CH$_2$)$_4$CH$_3$), 29.1 (d, CH$_2$CH$_2$CH$_2$PPh$_2$), 28.1 (d, CH$_2$CH$_2$CH$_2$PPh$_2$), 27.6 (d, CH$_2$CH$_2$CH$_2$PPh$_2$), 23.5 (s, FeCH$_2$(CH$_2$)$_4$CH$_3$), 23.3 (s, FeCH$_2$(CH$_2$)$_4$CH$_3$), 5.5 ppm (s, FeCH$_2$(CH$_2$)$_4$CH$_3$); ^{31}P NMR (120 MHz, CDCl$_3$): δ = −14.6 ppm; FTIR: $\tilde{v}$ = 1997, 1935 cm^{-1}; MS (ESI): m/z: 489.33 [M+H]$^+$; elemental analysis calcd (%) for C$_{28}$H$_{33}$FeO$_2$P (488.38): C 68.86, H 6.81 Fe 11.43; found: C 68.75, H 7.46, Fe 11.54.

Migration insertion polymerization (MIP) of 1: Bulk MIP of **1** (**1a**: R=CH$_3$, **1b**: R=(CH$_2$)$_5$CH$_3$, 1.0 mmol) was performed at either 70 or 105 °C. After polymerization, the crude product was dissolved in THF (5.0 mL) and was then precipitated with n-hexane (200 mL). The precipitate was collected by filtration and was dried under vacuum overnight at room temperature to yield a yellow powder (>90 %). Solution MIP of **1b** was performed in THF with a monomer concentration of 50 wt %. The solution was heated in an oil bath at 70 °C. After polymerization, the mixture was concentrated to 5.0 mL and then precipitated with n-hexane (200.0 mL). The precipitate was collected by filtration and dried under vacuum overnight at room temperature to yield a yellow powder. Yield for the final product with CH$_3$ or (CH$_2$)$_5$CH$_3$ is about 81 %.

Compound 2a: ^{1}H NMR (300 MHz, C$_6$D$_6$): δ = 7.80–7.30 (br, 5H, C$_6$H$_5$), 7.30–6.90 (br, 5H, C$_6$H$_5$), 4.20–3.90 (m, 4H, C$_5$H$_4$), 2.70–2.30 (m, 4H, CH$_2$CH$_2$CH$_2$PPh$_2$ and CH$_2$CH$_2$CH$_2$PPh$_2$), 2.30–2.00 (s, 3H, Fe(CO)CH$_3$), 1.63–1.20 ppm (s, 2H, CH$_2$CH$_2$CH$_2$PPh$_2$); ^{13}C NMR (75 MHz, C$_6$D$_6$): δ = 273.1 (C=O), 221.1 (C≡O), 102.6 (s, C$_5$H$_4$), 86.8 (s, C$_5$H$_4$), 84.5 (s, C$_5$H$_4$), 82.3 (s, C$_5$H$_4$), 51.7 (s, Fe(CO)CH$_3$), 29.7 (b, CH$_2$CH$_2$CH$_2$PPh$_2$, CH$_2$CH$_2$CH$_2$PPh$_2$), 26.1 ppm (s, CH$_2$CH$_2$CH$_2$PPh$_2$); ^{31}P NMR (120 MHz, CDCl$_3$): δ = 73.6 ppm; FTIR: $\tilde{v}$ = 1907 (terminal CO group), 1594 cm^{-1} (acyl CO group).

Compound 2b: ^{1}H NMR (300 MHz, C$_6$D$_6$): δ = 7.80–7.00 (br, 10H, C$_6$H$_5$), 4.20–3.80 (m, 4H, C$_5$H$_4$), 3.00 (s, 1H, Fe(CO)CH$_2$(CH$_2$)$_4$), 2.90 (s, 1H, Fe(CO)CH$_2$(CH$_2$)$_4$), 2.60–2.30 (t, 2H, CH$_2$CH$_2$CH$_2$PPh$_2$), 2.30–2.10 (m, 2H, CH$_2$CH$_2$CH$_2$PPh$_2$), 1.80–1.50 (t, 2H, CH$_2$CH$_2$CH$_2$PPh$_2$), 1.50–1.20 (s, 8H, Fe(CO)CH$_2$(CH$_2$)$_4$CH$_3$), 1.00–0.90 ppm (s, 3H, Fe(CO)CH$_2$(CH$_2$)$_4$CH$_3$); ^{13}C NMR (75 MHz, C$_6$D$_6$): δ = 273.9 (C=O), 220.7 (C≡O), 102.3 (s, C$_5$H$_4$), 86.7 (s, C$_5$H$_4$), 84.7 (s, C$_5$H$_4$), 82.1 (s, C$_5$H$_4$), 66.5 (s, Fe(CO)CH$_2$(CH$_2$)$_4$), 32.4 (s, Fe(CO)CH$_2$(CH$_2$)$_4$CH$_3$), 29.7 (br, CH$_2$CH$_2$CH$_2$PPh$_2$, CH$_2$CH$_2$CH$_2$PPh$_2$, Fe(CO)CH$_2$(CH$_2$)$_4$CH$_3$), 26.5 (s, Fe(CO)CH$_2$(CH$_2$)$_4$CH$_3$), 26.1 (s, CH$_2$CH$_2$CH$_2$PPh$_2$), 23.1 (s, Fe(CO)CH$_2$(CH$_2$)$_4$CH$_3$), 14.4 ppm (s, Fe(CO)CH$_2$(CH$_2$)$_4$CH$_3$); ^{31}P NMR (120 MHz, CDCl$_3$): δ = 73.6 pm; FTIR: $\tilde{v}$ = 1906 (terminal CO group), 1601 cm^{-1} (acyl CO group).

Acknowledgements

Conflict of interest

The authors declare no conflict of interest.

[1] a) C. Narayanan, N. D. Bernard, N. Doucet, *Catalysts* **2016**, *6*, 81; b) T. L. Aboye, J. A. Camarero, *J. Biol. Chem.* **2012**, *287*, 27026–27032; c) J. A. Semlyen, *Large Ring Molecules*, Wiley, New York, **1996**.

[2] a) J. Blankenstein, J. Zhu, *Eur. J. Org. Chem.* **2005**, 1949–1964; b) R. M. Kohli, C. T. Walsh, M. D. Burkart, *Nature* **2002**, *418*, 658; c) C. J. White, A. K. Yudin, *Nat. Chem.* **2011**, *3*, 509.

[3] a) H. Oike, M. Hamada, S. Eguchi, Y. Danda, Y. Tezuka, *Macromolecules* **2001**, *34*, 2776–2782; b) D. Aoki, G. Aibara, S. Uchida, T. Takata, *J. Am. Chem. Soc.* **2017**, *139*, 6791–6794.

[4] a) A. K. Yudin, *Chem. Sci.* **2015**, *6*, 30–49; b) V. Martí-Centelles, M. D. Pandey, M. I. Burguete, S. V. Luis, *Chem. Rev.* **2015**, *115*, 8736–8834.

[5] a) T. Yamamoto, S. Yagyu, Y. Tezuka, *J. Am. Chem. Soc.* **2016**, *138*, 3904–3911; b) *Topological Polymer Chemistry: Progress of Cyclic Polymers in Syntheses, Properties, and Functions* (Ed.: Y. Tezuka), World Scientific: Singapore, **2013**; c) H. R. Kricheldorf, *J. Polym. Sci. Part A* **2010**, *48*, 251–284.

[6] a) D. Cho, K. Masuoka, K. Koguchi, T. Asari, D. Kawaguchi, A. Takano, Y. Matsushita, *Polym. J.* **2005**, *37*, 506; b) S. Singla, T. Zhao, H. W. Beckham, *Macromolecules* **2003**, *36*, 6945–6948; c) C. N. Alexandru-Crivac, L. Dalponte, W. E. Houssen, M. Idress, M. Jaspars, K. A. Rickaby, L. Trembleau, *Cyclic Peptides: From Bioorganic Synthesis to Applications*, RSC, Cambridge, **2018**.

[7] a) C. W. Bielawski, D. Benitez, R. H. Grubbs, *Science* **2002**, *297*, 2041–2044; b) K. Zhang, M. A. Lackey, Y. Wu, G. N. Tew, *J. Am. Chem. Soc.* **2011**, *133*, 6906–6909.

[8] D. E. Herbert, J. B. Gilroy, W. Y. Chan, L. Chabanne, A. Staubitz, A. J. Lough, I. Manners, *J. Am. Chem. Soc.* **2009**, *131*, 14958–14968.

[9] a) P. J. Stang, B. Olenyuk, *Acc. Chem. Res.* **1997**, *30*, 502–518; b) Y.-T. Chan, X. Li, M. Soler, J.-L. Wang, C. Wesdemiotis, G. R. Newkome, *J. Am. Chem. Soc.* **2009**, *131*, 16395–16397.

[10] a) J. Liu, K. Cao, B. Nayyar, X. Tian, X. Wang, *Polym. Chem.* **2014**, *5*, 6702–6709; b) X. Wang, K. Cao, Y. Liu, B. Tsang, S. Liew, *J. Am. Chem. Soc.* **2013**, *135*, 3399–3402.

[11] H. Jiang, D. Geng, D. Liu, N. Lanigan, X. Wang, *Chem. Eur. J.* **2017**, *23*, 8280–8285.

[12] K. Cao, B. Tsang, Y. Liu, D. Chelladural, W. P. Power, X. Wang, *Organometallics* **2014**, *33*, 531–539.

[13] K. Cao, J. Ward, R. C. Amos, M. G. Jeong, K. T. Kim, M. Gauthier, D. Foucher, X. Wang, *Chem. Commun.* **2014**, *50*, 10062–10065.

[14] J. Liu, Z. Guan, X. Tian, J. Lin, X. Wang, *Polym. Chem.* **2016**, *7*, 4419–4426.

[15] K. Cao, X. Wang, *Macromol. Rapid Commun.* **2016**, *37*, 246–250.

[16] E. W. Abel, N. J. Long, K. G. Orrell, A. G. Osborne, V. Šik, *J. Organomet. Chem.* **1991**, *403*, 195–208.

[17] J. K. Stille, C. Smith, O. P. Anderson, M. M. Miller, *Organometallics* **1989**, *8*, 1040–1047.

[18] L. D. Quin, *A Guide to Organophosphorus Chemistry*, Wiley, Hoboken, **2000**.

[19] N. Murshid, X. Wang, *Chem. Eur. J.* **2015**, *21*, 19223–19230.

[20] D. A. Foucher, C. H. Honeyman, J. M. Nelson, B. Z. Tang, I. Manners, *Angew. Chem. Int. Ed. Engl.* **1993**, *32*, 1709–1711; *Angew. Chem.* **1993**, *105*, 1843–1845.

[21] M. Schappacher, A. Deffieux, *Science* **2008**, *319*, 1512–1515.

[22] K. Zhang, Y. Zha, B. Peng, Y. Chen, G. N. Tew, *J. Am. Chem. Soc.* **2013**, *135*, 15994–15997.

[23] S. M. Mukhopadhyay, in *Sample Preparation for Microscopic and Spectroscopic Characterization of Solid Surfaces and Films*, Wiley, **2003**, pp. 377–411.

[24] a) J. des Cloizeaux, *J. Phys. Lett.* **1981**, *42*, 433–436; b) J. A. Semlyen, *Cyclic Polymers*, Springer, **2000**.

[25] C. D. Roland, H. Li, K. A. Abboud, K. B. Wagener, A. S. Veige, *Nat. Chem.* **2016**, *8*, 791–796.

[26] Z. Jia, M. J. Monteiro, *J. Polym. Sci. Part A* **2012**, *50*, 2085–2097.

[27] a) T. Josse, J. De Winter, P. Gerbaux, O. Coulembier, *Angew. Chem. Int. Ed.* **2016**, *55*, 13944–13958; *Angew. Chem.* **2016**, *128*, 14150–14164; b) Q. Tang, J. Chen, Y. Zhao, K. Zhang, *Polym. Chem.* **2015**, *6*, 6659–6663.

[28] a) Y. Zhu, N. S. Hosmane, *ChemistryOpen* **2015**, *4*, 408–417; b) W. Chen, Y. Zhou, Y. Li, J. Sun, X. Pan, Q. Yu, N. Zhou, Z. Zhang, X. Zhu, *Polym. Chem.* **2016**, *7*, 6789–6797; c) X.-Y. Tu, M.-Z. Liu, H. Wei, *J. Polym. Sci. Part A* **2016**, *54*, 1447–1458.